Calculation of electron-impact rotationally elastic total cross sections for NH_3, H_2S, and PH_3 over the energy range from 0.01 eV to 2 keV

Chetan Limbachiya,[1] Minaxi Vinodkumar,[2,*] and Nigel Mason[3]
[1]*P. S. Science College, Kadi 382 715, Gujarat, India*
[2]*V. P. and R. P. T. P. Science College, Vallabh Vidyanagar 388 120, Gujarat, India*
[3]*Department of Physics and Astronomy, Open University, Milton Keynes, MK7 6AA, UK*
(Received 2 December 2010; published 18 April 2011)

This paper report results of calculation of the total cross section Q_T for electron impact on NH_3, H_2S, and PH_3 over a wide range of incident energies from 0.01 eV to 2 keV. Total cross sections Q_T (elastic plus electronic excitation) for incident energies below the ionization threshold of the target were calculated using the UK molecular *R*-matrix code through the Quantemol-N software package and cross sections at higher energies were derived using the spherical complex optical potential formalism. The two methods are found to give self-consistent values where they overlap. The present results are, in general, found to be in good agreement with previous experimental and theoretical results.

DOI: 10.1103/PhysRevA.83.042708 PACS number(s): 34.80.Bm

I. INTRODUCTION

Electron molecule collisions are important over all ranges of incident energy starting from very low impact energies (0.01 eV) to intermediate and high energies (10 keV). Low-energy collision processes are perhaps the most important processes to understand since they underpin the physicochemical processes prevalent in plasmas and many industrial discharges. At low energies (<10 eV) electrons may also form short-lived anions (resonances) whose decay (to produce neutral and anionic fragments) may strongly influence the local chemistry. Theoretical predictions of low-energy resonance formation are strongly linked to a detailed knowledge of the forces acting on the electrons during the scattering process and are a consequence of the structural properties of the target. On the other hand, intermediate to high-energy electron-scattering cross sections are required in astrophysics, atmospheric physics, and radiation physics often where high-energy-radiation x rays, cosmic rays, and the like interact with targets to produce an avalanche of lower-energy secondary electrons. Accordingly there is a need for total scattering cross sections over a wide energy range from meV to MeV.

In this paper we present rotationally elastic total cross sections for electron scattering from three molecules (NH_3, H_2S, and PH_3) chosen to demonstrate the possibility of producing robust cross sections over a wide energy range (from 0.01 eV to 2 keV) using two different theoretical formalisms that may be adopted for any target. We use the commercial Quantemol-N formalism for calculating total (elastic plus electronic excitation) cross sections up to threshold of the target and the Spherical Complex Optical Potential method for calculating total (elastic plus inelastic) cross sections beyond a threshold up to 2 keV [1]. We do not claim that the resultant cross sections are the most accurate but rather wish to show that it is practical to supply a self-consistent set of cross sections over this wider energy range such that such data may be supplied to any "data user" quickly and easily. We have selected these three molecules since they have a simple molecular geometry and a modest number of total electrons making the calculations computationally faster and because these three compounds have been studied extensively, both experimentally and theoretically, allowing us to benchmark our methodology.

Electron collisions with NH_3 are important in interstellar space [2], and NH_3 is a major component of the Jovian [3] and Saturnian [4] atmospheres. In the field of plasma chemistry, NH_3 is used as the source of nitrogen atoms for the fabrication of nitride films and other nitrogen compounds. Electron-impact total cross sections for NH_3 have been measured at low energies by Jones *et al.* (0.02–10 eV) [5], Szmytkowski *et al.* (1–80 eV) [6], Bruche (2–20 eV) [7], and Alle *et al.* (2–30 eV) [8], and at intermediate and high energies by Zecca *et al.* (75–4000 eV) [9], Sueoka *et al.* (1–400 eV) [10], Garcia and Manero (300–5000 eV) [11], and Ariyasinghe *et al.* (400–4000 eV) [12]. Compared to these extensive experimental studies, theoretical calculations of the total electron-scattering cross section are sparse. Munjal and Baluja (0.025–20 eV) [13] have reported low-energy elastic cross sections using the *R* matrix, Gianturco (1–20 eV) [14] has reported total elastic cross sections using *ab initio* calculations, while Yuan and Zhang have reported total cross sections in the range 0.5–20 eV [15]. Intermediate and high-energy calculations have been reported by Liu *et al.* (10–1000 eV) [16] and Jain (10–3000 eV) [17].

H_2S is a well-known toxic gas that when present in high concentrations is fatal to all forms of life. It has recently been observed in comets [18] and in the Orion Plateau [19]. Electron-impact total cross sections for H_2S have been measured at low energies by Jones *et al.* (0.02–10 eV) [5], Gulley *et al.* (1–30 eV) [20], and Sokolov and Sokolova (0–10 eV) [21], and at low to high energy by Szmytkowski *et al.* (6–370 eV) [22] and Zecca *et al.* (75–4000 eV) [9]. Low-energy calculations were carried out by Varella *et al.* (5–30 eV) [23] using the Schwinger multichannel method and by Gupta and Baluja (0.025–15 eV) [24] using the *R*-matrix code. Lengsfield *et al.* [25] have also reported data in the energy range 1–30 eV. Intermediate- to high-energy

*minaxivinod@yahoo.co.in

TABLE I. Properties of target: ground-state energy (hartree), dipole moment (a.u.), first excitation energy (eV), and rotational constant (cm^{-1}).

	Ground-state energy (hartree)		Dipole moment (a.u.)			First excitation energy E_1 (eV)			Rotational constant (B) (cm^{-1})	
Target	Present	Theo.	Present	Theo.	Expt.	Present	Theo.	Expt.	Present	Theo.
NH_3	−56.19	56.45 [54]	0.832	0.611 [13] 0.648 [14]	0.578 [56]	6.89	7.78 [13]	—	9.97	9.44 [59] 9.94 [26]
H_2S	−398.69	398.9 [54]	0.509	0.782 [23] 0.431 [55]	0.384 [56]	6.26	6.7 [24] 5.88 [57] 6.17 [58]	6.3 [56]	10.48	8.99 [59] 10.36 [26]
PH_3	−342.47	342.6 [54]	0.313	0.311 [32] 0.225 [56]	0.225 [56]	6.42	—	—	4.44	4.45 [58] 4.45 [26]

calculations have been reported by Jain and Baluja (10–5000 eV) [26] and Shi *et al.* (30–5000 eV) [27].

PH_3 is widely used as a source of phosphorous to produce high-quality thin film of InP and GaP [28], and it is now used in the manufacturing of devices for quantum computing [29]. Recently it has also been detected in the troposphere of giant planets [30]. Total cross sections for PH_3 have been measured by Szmytkowski *et al.* (0.5–370 eV) [31] using the linear transmission method, and calculations of electron-impact total cross sections have been reported by Jain and Baluja (10–5000 eV) [26], Munjal and Baluja (0.025–15 eV) [32], and Bettega *et al.* (1–10 eV) [33].

We have listed in Table I the ground-state energy, the first electronic excitation energy, the dipole moment, and rotational constants of the target obtained through the calculations, and these are compared with available theoretical and experimental data wherever possible. The present results for ground-state energy are in excellent agreement with the previous theoretical calculations, which further signifies the good selection of the basis set to represent the target wave function. Our calculated rotational constants and the first electronic excitation energies also agree well with the data in the literature. The present value of dipole moment also compares fairly well with available data, as is evident from Table I. Vertical excitation energies for different electronic states are shown in Table II

II. THEORETICAL METHODOLOGY

As mentioned earlier, over such a vast range of incident energy it is not possible to use a single theoretical formalism. Hence low-energy calculations (0.01 to ≈15 eV) were performed using an *ab initio* *R*-matrix methodology through the Quantemol-N software while at higher energies we employed the well-established Spherical Complex Optical Potential (SCOP) method [34]. The theoretical methodology is therefore described in two subsections: (1) the low-energy formalism and (2) the high-energy formalism. However, before we discuss the scattering dynamics it is necessary to describe the molecular target.

A. Target description

The ammonia molecule has a trigonal pyramidal shape with a bond angle of 107.8°. NH_3 is formed by bonding each of the three unpaired 1*s* orbitals of hydrogen with three unpaired 2*p* orbitals of nitrogen. In our formalism we have used the Gaussian basis set 6-311G. Here six Gaussians are used to sum up inner shell orbitals, three Gaussians for the first Slater-type orbitals (STOs) of the valence orbitals, and one Gaussian for the second and third STOs of the valence orbitals. NH_3 has three symmetrically nonredundant atoms and

TABLE II. Vertical excitation energies in eV.

NH_3		H_2S		PH_3	
State	Energy (eV)	State	Energy (eV)	State	Energy (eV)
$^3A'$	6.89	$^3A''$	6.26	$^3A'$	6.53
$^1A'$	7.29	$^1A''$	6.81	$^3A''$	6.53
$^3A''$	9.12	$^3B'$	7.37	$^1A''$	8.60
$^3A'$	9.12	$^1B'$	8.39	$^1A'$	8.60
$^1A''$	9.49	$^3B''$	8.57	$^3A'$	9.79
$^1A'$	9.49	$^3A'$	9.92	$^3A'$	10.45
$^3A''$	12.33	$^1B''$	11.39	$^3A''$	10.45
$^3A'$	12.33	$^1A'$	11.58	$^3A''$	10.99
$^1A''$	13.02	$^3A'$	11.79	$^1A'$	11.22
$^1A'$	13.02	$^3B''$	12.35	$^1A''$	12.35
$^3A'$	13.93	$^1B''$	14.46	$^1A'$	12.36
$^3A''$	14.63	$^1A'$	14.50	$^1A'$	12.73
$^3A''$	14.98	$^1A'$	15.90	$^3A''$	15.62
$^1A''$	15.29	$^3B''$	16.00	$^1A''$	16.56
$^1A''$	15.47	$^3B'$	16.29	$^3A''$	16.95
		$^3A''$	17.21		
		$^3A''$	17.57		
		$^1B'$	17.81		
		$^1A''$	17.92		
		$^3A''$	17.93		
		$^3B'$	18.08		
		$^1B''$	18.47		
		$^1A''$	18.55		
		$^3B'$	18.86		
		$^3B''$	20.03		
		$^1B''$	20.22		
		$^3A'$	20.34		
		$^1A''$	20.46		
		$^1B'$	20.63		
		$^1B'$	21.33		
		$^3A\prime$	21.83		

has a C_s point group. The ground-state electronic configuration is $1a_1^2$, $2a_1^2$, $3a_1^2$, $1a_2^2$, $4a_1^2$. We have frozen two electrons in the $1a_1$ molecular orbital and kept eight valence electrons in the active space of seven molecular orbitals ($2a_1$, $3a_1$, $4a_1$, $5a_1$, $6a_1$, $1a_2$, $2a_2$). To improve the representation of the excited states, we used the molecular orbitals obtained from a Hartree-Fock selfconsistent field calculation to build state-averaged pseudonatural orbitals (NOs). Configuration integration (CI) calculations were performed for the states included in the close-coupling expansion. Then a weighted average of the density matrices obtained from these states was produced, and the NOs were obtained from its diagonalization. The total number of generated configuration state functions (CSF's) for the ground state was 2688, and the number of channels included in the calculation was 200. With the NOs and complete active space CI model mentioned above and using the GAUSPROP and DENPROP modules [35] of the R matrix, which are present in the target section of the code, the ground-state energy was −56.19 hartree, the dipole moment was 0.830 a.u., and 15 electronic excitation thresholds were found to be as listed in Table II.

H_2S is a trigonal planar bent molecule with a bond angle of 92.11°. H_2S is formed by bonding each of the two unpaired $1s$ orbitals of hydrogen with two unpaired $3p$ orbitals of sulfur. We have used a double-zeta-plus polarization (DZP) basis set for our calculations. The double-zeta basis set is important because it allows us to treat each orbital separately when we conduct the Hartee-Fock calculation. This gives us a more accurate representation of each orbital. H_2S has symmetrically two nonredundant atoms and has a C_{2V} point group. The Hartree-Fock electronic configuration of the ground state is $1a_1^2$, $2a_1^2$, $1b_2^2$, $3a_1^2$, $1b_1^2$, $4a_1^2$, $2b_2^2$, $5a_1^2$, $2b_1^2$. Out of total 18 electrons, we have frozen 10 electrons in five molecular orbitals—$1a_1$, $2a_1$, $3a_1$, $1b_1$, and $1b_2$—and eight electrons are kept in an active space of eight molecular orbitals ($4a_1$, $5a_1$, $6a_1$, $7a_1$, $2b_1$, $2b_2$, $3b_2$, $4b_2$). The total number of generated CSF's for the ground state is 508, and the number of channels included in the calculation is 200. The GAUSPROP and DENPROP modules [35] yield ground-state energy of −398.69 hartree, a dipole moment of 0.509 a.u., and 31 electronic excitation thresholds as listed in Table II.

PH_3 has trigonal pyramidal geometry with a bond angle of 93.34°. PH_3 is formed by bonding each of the three unpaired $1s$ orbitals of hydrogen with unpaired $3p$ orbitals of phosphorous. We have used a DZP basis set for our calculation. PH_3 has symmetrically three nonredundant atoms and a C_s point group. The Hartree-Fock electronic configuration of the ground state is $1a_1^2$, $2a_1^2$, $1a_2^2$, $3a_1^2$, $4a_1^2$, $5a_1^2$, $6a_1^2$, $2a_2^2$, and $7a_1^2$. Out of a total of 18 electrons we have frozen 10 electrons in five molecular orbitals—$1a_1$, $2a_1$, $3a_1$, $4a_1$, and $1a_2$—while eight electrons are kept in the active space of seven molecular orbitals ($5a_1$, $6a_1$, $7a_1$, $8a_1$, $9a_1$, $2a_2$, $3a_2$). The total number of generated CSF's for the ground state was 260, and the number of channels included in the calculation was 200. These target properties listed in the Table I are one of the inputs for the outer region calculations. The ground-state energy obtained is −342.47 hartree, the dipole moment 0.313 a.u., and the lowest 15 electronic excitation thresholds are listed in Table II.

B. Low-energy formalism (0.01–15 eV)

The R-matrix method [36,37] is perhaps the most widely used method for calculating low-energy electron-molecule-scattering cross sections. In this paper we have used UK molecular R-matrix codes as available in the commercially Quantemol-N software [38]. The basic details of the underlying principles and methodology are briefly reviewed below.

The basic idea of the R-matrix method is the partitioning of configuration space into inner region and outer regions. The boundary of these two regions is selected such that the electronic charge cloud of the target is negligible at the boundary. In the present case for NH_3, H_2S, and PH_3 we have taken it to be a sphere of radius $10a_o$ centered at the center of mass of the molecule. Generally the radius is chosen in such a way that the electronic density of all the target states included in the calculation is negligible outside the sphere. In the inner region the scattering electron is indistinguishable from the electrons of the target, and short-range interactions of exchange and polarization are dominant. In the inner region quantum chemistry methods are employed to solve the N+1 eigenvalue problem. When the scattering electron is at a large distance from the center of mass of the target, the probability of such interactions is negligible, thereby simplifying the problem in the outer region considerably, and the scattered electron is assumed to propagate in the multipole potential of the target.

In the inner region, the wavefunction is constructed using the close coupling approximation [39], which is common to other *ab initio* calculations, and accordingly it is written as

$$\psi_k^{N+1} = A\sum_i \Phi_i^N(x_1,x_2,\ldots,x_N)\sum_j \xi_j(x_{N+1})a_{ijk} + \sum_m \chi_m(x_1,x_2,\ldots.x_{N+1})b_{mk}, \quad (1)$$

where A is an antisymmetrization operator, x_N is the spatial and spin coordinate of the N^{th} electron, Φ_i^N is the ith state of the N-electron target that is represented using a CI expansion, and ξ_j is a continuum orbital spin coupled with the target states. The coefficients a_{ijk} and b_{mk} are variational parameters that can be determined by solving the $N+1$ eigenvalue problem in the inner region by employing standard bound-state quantum chemistry methods. The standard way of performing a CI target calculation is to use a complete active space CI (CASCI) as this model keeps a balance between the target and scattering calculations. In this model valence electrons are freely distributed among the subsets of the valence orbitals.

The occupied and virtual target molecular orbitals are constructed using the Hartree-Fock self-consistent field method with Gaussian-type orbitals (GTOs) and the continuum orbitals of Faure *et al.* [40] and include up to g ($l = 4$) orbitals. The advantage of using Gaussian-type orbitals is that infinite-range integrals are evaluated exactly. In practice all the integrals are evaluated in the entire configuration space, and the tail contribution outside the R-matrix sphere is then subtracted. This can be done efficiently using property integrals for the short-range GTOs. However, treating a large number of coupled states makes the outer region calculations slow since the open-closed portion of the R-matrix at the spherical

boundary becomes larger. To overcome this problem most of the strongly closed channels are omitted from the outer region. This technique gives excellent results provided all open states and a few of closed ones are retained in the outer region [41].

After generating the wave functions, using Eq. (1), their eigenvalues are determined. The R matrix is constructed at the boundary between the inner and outer regions for a chosen set of incident energies. Finally the R matrix is propagated to an asymptotic region where the radial wavefunction describing the scattering electron can be matched to an analytical expression, from which K-matrix elements are determined, and subsequently the resonance positions, widths, and cross sections are computed using T matrix.

The R matrix has a number of distinct advantages, a major one being that the given basis set can span the appropriate energy range, the inner region problem needs to be solved only once, and the energy dependence is obtained entirely from the solution of the simpler outer region problem. Another advantage is that it can generate large numbers of energies at little extra computational cost. [42]

C. Higher-energy formalism (15 eV–2 keV)

Since Quantemol-N makes use of the R-matrix code it is limited to the calculation of cross sections below the ionization threshold of the molecule being considered. Beyond the ionization threshold of the target we performed scattering calculations using the well-established SCOP formalism [43–45], which yields the total elastic cross section $Q_{\rm el}$ and its counterpart the total inelastic cross sections $Q_{\rm inel}$ such that the total scattering cross section (TCS) Q_T is given by

$$Q_T(E_i) = Q_{\rm el}(E_i) + Q_{\rm inel}(E_i). \tag{2}$$

Our calculation for these TCSs is based on complex scattering potentials, generated from spherically averaged charge densities of the target. The charge density of lighter hydrogen atoms is expanded at the center of heavier atom (nitrogen, sulfur, or phosphorous) by employing the Bessel function expansion as by Gradshetyn and Ryzhik [46]. This is a good approximation since hydrogen atoms do not significantly act as scattering centers, and the cross sections are dominated by the central atom size. Thus, the single-center molecular charge density is obtained by a linear combination of constituent atomic charge densities, renormalized to account for covalent molecular bonding. The molecular charge density is employed to construct a complex optical potential $V_{\rm opt}$, given by

$$V_{\rm opt}(E_i,r) = V_R(E_i,r) + iV_I(E_i,r). \tag{3}$$

The real part V_R comprises static potential ($V_{\rm st}$), exchange ($V_{\rm ex}$), and polarization (V_p) terms, as follows:

$$V_R(E_i,r) = V_{\rm st}(r) + V_{\rm ex}(E_i,r) + V_P(E_i,r). \tag{4}$$

We have used the analytical form of the static potential derived using the Hartree-Fock wavefunctions of Bunge *et al.* [47]. For the exchange potential, we have used Hara's parameter-free "free electron gas exchange model" [48], and for the polarization potential V_p, we have used a parameter-free model of the correlation polarization potential that contains multipole nonadiabatic corrections in the intermediate region and smoothly approaches the correct asymptotic form for large r given by Zhang *et al.* [49]. The imaginary part V_I, also called the absorption potential $V_{\rm abs}$, accounts for the total loss of scattered flux into all the allowed channels of electronic excitation and ionization. For $V_{\rm abs}$ we have used the model potential given by Staszeweska *et al.* [50], which is a quasifree, Pauli-blocking, dynamic absorption potential. The form of the potential is given as

$$V_{\rm abs}(r,E_i) = -\rho(r)\sqrt{\frac{T_{\rm loc}}{2}}\left(\frac{8\pi}{10k_{F^3}E_i}\right) \times \theta(p^2 - k_{F^2} - 2\Delta)(A_1 + A_2 + A_3). \tag{5}$$

The parameters A_1, A_2, and A_3 are defined as under

$$A_1 = 5\frac{k_f^3}{2\Delta}, \quad A_2 = \frac{k_f^2\left(5p^2 - 3k_f^2\right)}{\left(p^2 - k_f^2\right)^2}, \quad \text{and}$$

$$A_3 = \frac{2\theta\left(2k_f^2 + 2\Delta - p^2\right)\left(2k_f^2 + 2\Delta - p^2\right)^{5/2}}{\left(p^2 - k_f^2\right)^2},$$

and the local kinetic energy of the incident electron is given by

$$T_{\rm loc} = E_i - (V_{\rm st} + V_{\rm ex}). \tag{6}$$

The absorption potential is a function of the molecular charge density [$\rho(r)$], the incident energy (E_i), and the parameter Δ of the target. It is not sensitive to long-range potentials such as $V_{\rm pol}$ and hence is neglected in the local kinetic energy term of Eq. (6). In Eq. (5), $p^2 = 2E_i$, is the energy of incident electron in hartrees, and $k_F = [3\pi^2\rho(r)]^{1/3}$ is the Fermi wavevector. $\theta(x)$ is the Heaviside unit step function, such that $\theta(x) = 1$ for $x \geqslant 0$, and is zero otherwise. The dynamic functions A_1, A_2, and A_3 of Eq. (5) depend upon $\rho(r)$, I, Δ, and E_i. The parameter Δ determines a threshold below which $V_{\rm abs} = 0$, and the ionization or excitation is prevented energetically. So in order to include excitations due to discrete levels at lower energy, we have considered Δ as an energy-dependent parameter. Hence, Δ as a variable accounts for more penetration of the absorption potential in the target charge-cloud region. Below the ionization threshold of the target, the value of Δstarts with $0.8I$ and slowly reaches to the value I at the peak of inelastic cross section [51–53]. We express Δ as a function of E_i around I as

$$\Delta(E_i) = 0.8I + \beta(E_i - I). \tag{7}$$

Here β is obtained by requiring that $\Delta = I$ at $E_i = E_p$, where E_p is the value of E_i at which $Q_{\rm inel}$ attains maximum value. For $E_i > E_p$, Δ is held constant and equal to the ionization energy of the target as suggested in the original model of Staszeweska *et al.* [50]. The choice of $\Delta = $ I throughout the incident energy range would reject the electronic excitation at $E_i \leqslant I$. On the other hand, if parameter Δ is much less than the ionization threshold, then $V_{\rm abs}$ becomes exceedingly high because at low energies the cross sections are very sensitive to Δ variations.

After generating the full complex potential given in Eq. (3) for a given electron molecule system, we solve the Schrödinger equation numerically using partial wave analysis. In partial wave analysis we assume the potential to be central such that

it depends only on the radial distance r. Solving the radial part of the Schrödinger equation yields us complex phase shifts. This shift in the angle or the phase is the reflection of the interaction of the potential on the outgoing wave. Phase shifts are the key ingredients that carry all the information regarding the scattering event. Knowledge of phase shift is employed to compute the scattering amplitude given by

$$f(k,\theta) = \frac{1}{2ik}\sum_{l=0}^{\infty}(2l+1)[\exp(2i\delta_l)-1]P_l(\cos\theta). \quad (8)$$

This can be rewritten as

$$f(k,\theta) = \frac{1}{2ik}\sum_{l=0}^{\infty}(2l+1)[S_l(k)-1]P_l(\cos\theta), \quad (9)$$

where $S_l(k) = \exp(2i\delta_l)$ is the S-matrix (scattering matrix) elements. Using the phase shifts in the standard relations [53] of the various total cross sections is computed as in Eq. (2).

In Table I we have listed the ground-state energy, first electronic excitation energy, dipole moment, and rotational constant of the target obtained through the calculations and are compared with available theoretical and experimental data wherever possible.

As can be seen from Table I, although the present dipole moment shows fair agreement with available data, the ground-state energy, first electronic excitation energy, and rotational constant for all the present targets match extremely well with the compared data.

In Table II we have listed the vertical excitation energies for NH_3, H_2S, and PH_3 molecules for 15, 31, and 15 electronic excited states, respectively.

III. RESULTS AND DISCUSSION

In Table III we have listed numerical values of the total cross sections (in Å^2) for all the three targets over the energy range 0.1–2000 eV. The present results are also shown graphically for all the three selected molecular targets in Figs. 1–6 along with previous experimental and theoretical results. In order to maintain the clarity of the figures we have shown the comparisons for each target in two figures. Figure 1 shows the comparison with experimental data, and Figure 2 shows a comparison with theoretical data. It is observed that in general there is good agreement between the present results and all the available data over the entire incident energy range. The nature of the curves is very good for all the targets with minima and maxima of the cross sections reproduced at the same energies as predicted and measured by earlier authors. It should also be noted that the results obtained using the two methods (R-matrix and SCOP) match remarkably well at the transition energy (15 eV) while maintaining the shape and slope of the cross-section curve. The composite calculation is therefore capable of providing a data set for TCS that is both self-consistent and reliable. We will now discuss the results of each target in turn.

In Fig. 1 we compare our current electron NH_3-scattering cross sections over the complete range of incident energy (0.01–2000 eV) with previous experimental results. The total elastic cross sections including electronic excitations are computed and plotted below the ionization threshold with total cross sections obtained as the sum of elastic and inelastic cross sections plotted above ionization threshold. The present results are in fairly good agreement with the experimental data of Jones *et al.* [5], Bruche [7], Zecca *et al.* [9], Garcia *et al.* [11], and Ariyasinghe *et al.* [12]. In particular the present results are in very good agreement with the experimental results of Sueoka *et al.* [10] below 4 eV and above 100 eV, between 4 and 10 eV the present data are slightly lower than results of Sueoka *et al.* [10], while above 15 eV the present results are slightly higher. The minima reported by Sueoka *et al.* is 10.1 Å^2 at 2.5 eV, which is reproduced very well with our present calculated value being 11.6 Å^2 at the same energy. The experimental data of Szmytkowski *et al.* [6] are in good agreement with present results throughout the range except near the peak, where they are higher compared with other reported values. The experimental data of Alle *et al.* [8], produced by extrapolation and integration of the differential

TABLE III. Total cross sections (Å^2).

	Cross sections		
Energy(eV)	NH_3	H_2S	PH_3
0.1	176	191	11.41
0.2	104	90.6	10.39
0.4	53.8	42.0	10.63
0.6	34.8	27.0	11.27
0.8	25.6	20.4	11.99
01	20.5	17.1	12.77
1.5	14.7	15.1	15.16
02	12.5	19.6	19.66
03	11.3	29.0	43.30
04	11.7	25.4	43.51
05	12.8	26.6	39.47
06	14.0	27.9	38.22
07	15.1	28.5	38.87
08	16.2	28.6	37.86
09	16.9	28.5	41.01
10	17.3	28.2	39.48
11	17.4	27.8	37.12
12	17.5	27.2	35.85
13	17.1	26.4	34.72
14	16.8	25.7	33.76
15	16.2	24.9	32.90
20	15.74	23.7	29.60
30	14.66	20.36	24.46
40	13.25	17.62	20.64
80	09.54	12.19	14.24
100	08.47	10.95	12.76
200	05.71	07.64	08.70
300	04.42	06.01	06.72
400	03.64	05.00	05.54
500	03.10	04.32	04.74
600	02.71	03.82	04.17
700	02.41	03.43	03.74
800	02.17	03.13	03.40
900	01.98	02.88	03.12
1000	01.84	02.68	02.90
1500	01.35	02.01	02.15
2000	01.08	01.63	01.73

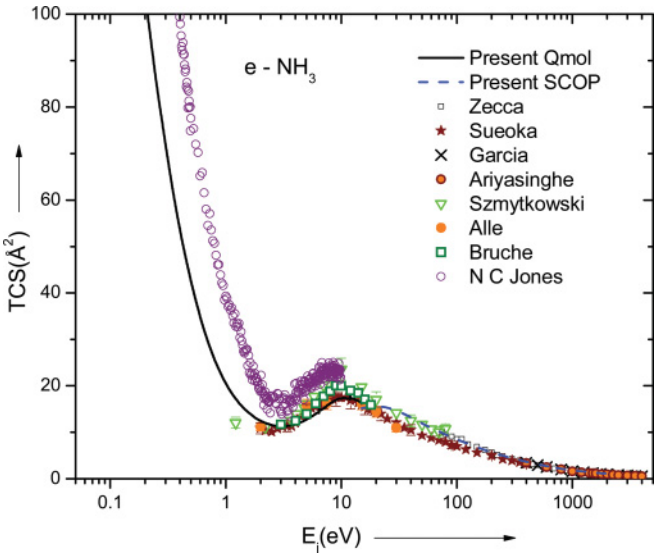

FIG. 1. (Color online) TCS for e-NH_3 scattering. Solid line (black) line, present TCS (using Qmol with excitation); dashed line (blue), present TCS using SCOP; squares, experimental data of Zecca *et al.* [9]; stars, experimental data of Sueoka *et al.* [10]; crosses, experimental data of Garcia *et al.* [11]; diamond (filled), experimental data of Ariyasinghe *et al.* [12]; inverted triangles, experimental data of Szmytkowski *et al.* [6]; filled circles, experimental data of Alle *et al.* [8]; open squares, experimental data of Bruche [7] ; open circles, experimental data of Jones *et al.* [5].

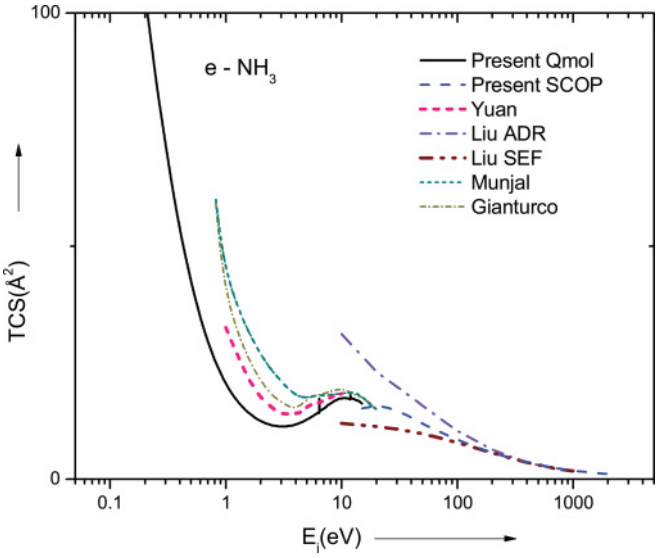

FIG. 2. (Color online) TCS for e-NH_3 scattering. Solid line (black) line, present TCS (using Qmol with excitation); dashed line (blue), present TCS using SCOP; pink dashed line, theoretical data of Yuan and Zhang [15]; violet dashed-dot line, theoretical data of Liu *et al.* using ADR method [16]; brown dashed-dot-dot line, theoretical data of Liu *et al.* using SEF method [16]; cyan dotted line, theoretical data of Munjal and Baluja [13] using ADR method; dark yellow short dash-dot line, Theoretical data of Gianturco [14].

cross sections, are in fair agreement with the present data. There are no experimental data reported for total cross sections below 0.5 eV, but our present results are lower than those of Jones *et al.* [5] below 1.3 eV.

In Fig. 2 we compare our recent results for e-NH_3 scattering with earlier reported theoretical data. Theoretical calculations have been reported by Manjul and Baluja [13] and Gianturco [14], and they agree well with the present results beyond 10 eV, but at lower energies these theoretical data are higher while maintaining the shape of the curve. Liu *et al.* [16] have reported total cross sections using two formalisms: one using an additivity rule that overestimates the cross section below 100 eV as expected and another using a semiempirical formula that is lower compared to all reported data below 30 eV. Both datasets of Liu *et al.* [16] agree well with present results beyond 200 eV. The theoretical results of Yuan and Zhang [15] are higher compared to all reported data below 100 eV, above which they are in excellent agreement with present results throughout the energy range they report.

In Fig. 3 we compare our total cross sections for e-H_2S scattering with available experimental data. Experimental results at very low energy (<1 eV) have been reported only by Jones *et al.* [5], and while we agree in the shape of the cross section at these low energies, we are slightly lower than the measured data until 2 eV, beyond which we agree very well with their data. Experimental data for low impact energy have also been reported by Szmytkowski *et al.* [22] and agree well with the present results beyond 30 eV, but below this energy the experimental data appear to be higher than calculations. In contrast the experimental data reported by Zecca *et al.* [9] at higher energy are in good agreement with present data throughout their reported energy range. The data of Gulley *et al.* [20] are also in good agreement with the present calculations.

In Fig. 4 we compare our present calculations for e-H_2S scattering with previous theoretical investigations. Very low-energy theoretical calculations have been reported by Gupta and Baluja [24] and Lengsfield *et al.* [25]. Low- to

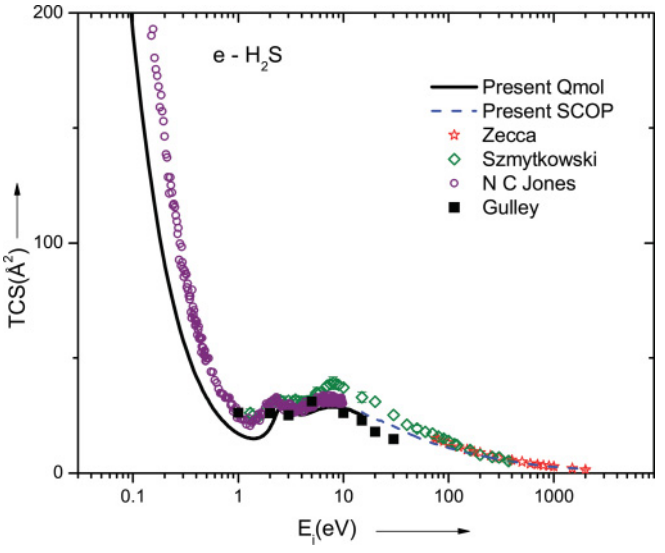

FIG. 3. (Color online) TCS for e-H_2S scattering. Solid line (black), present TCS using the Qmol formaliam); dash line (blue), recent TCS using the SCOP formalism; stars, experimental results of Zecca *et al.* [9]; open diamonds, experimental results of Szmytkowski *et al.* [22]; open circles, experimental results of Jones *et al.* [5]; filled squares, experimental results of Gulley *et al.* [20].

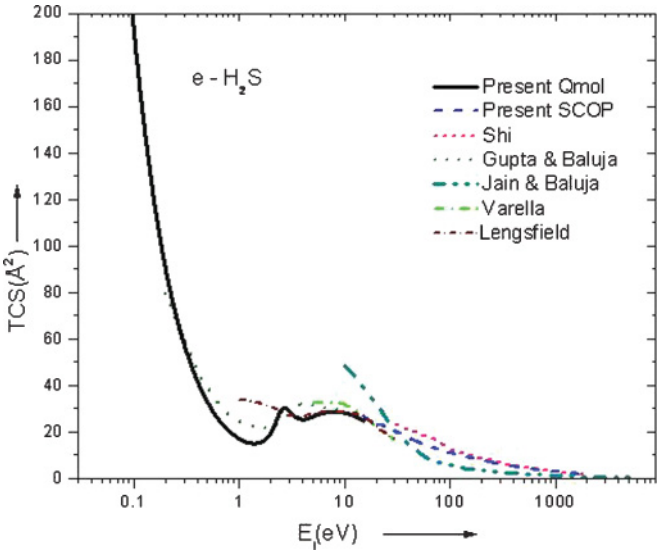

FIG. 4. (Color online) TCS for e-H_2S scattering. Solid line (black), present TCS using the Qmol formaliam); dash line (blue), present TCS using the SCOP formalism; pink short dash line, theoretical data of Shi *et al.* [27]; light pink dotted line, theoretical data of Gupta and Baluja [24]; dash-dot-dot line, theoretical data of Jain and Baluja [26]; long dash-dot line, theoretical data of Varella *et al.* [23]; short-dash-dot, theoretical data of Lengsfield *et al.* [25].

intermediate-energy calculations were reported by Varella *et al.* [23], Shi *et al.* [27], and Jain and Baluja [26]. The theoretical data of Gupta and Baluja [24] are in good accord with the present results with minima at the same energy (1.5 eV) as the present results. Below 0.5 eV they agree very well with present data, and between 3 to 5 eV their values are a little higher, but beyond 5 eV they once again agree with the present results. The theoretical data of Lengsfield *et al.* [25] show agreement with present results beyond 2 eV as observed in the case of NH_3, but below 2 eV their values are higher than our calculations. Varella *et al.* [23] used the Schwinger

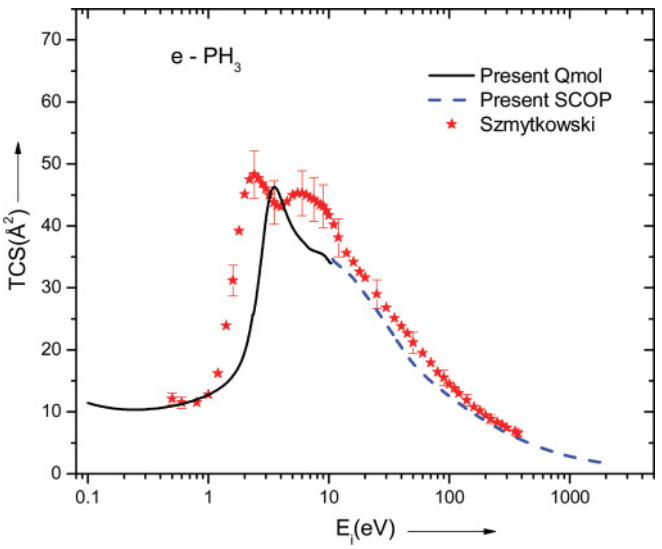

FIG. 5. (Color online) TCS for e-PH_3 scattering. Solid line (black), present TCS using Qmol; dash line (blue), present TCS using SCOP; stars, experimental results of Szmytkowski *et al.* [31].

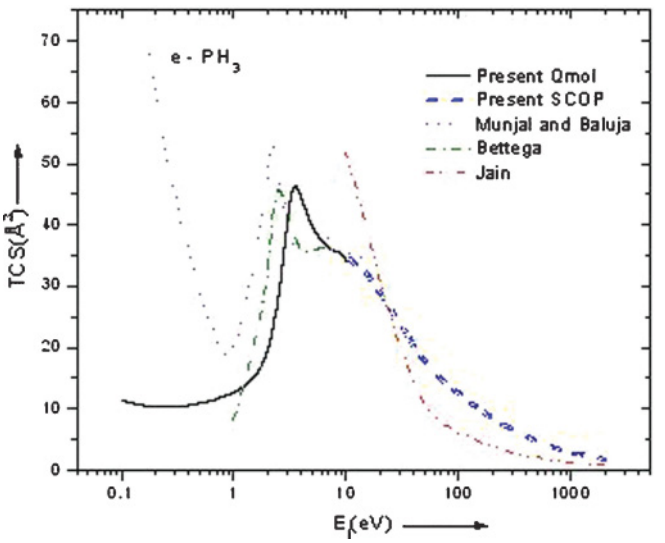

FIG. 6. (Color online) TCS for e-PH_3 scattering. Solid line (black), present TCS using Qmol; dash line (blue), present TCS using SCOP; short dash line, theoretical calculations of Munjal and Baluja [32]; dash-dot line, theoretical results of Bettega *et al.* [33]; dash-dot-dot line, theoretical calculations of Jain [26].

multichannel method with pseudopotentials to calculate elastic and rotationally inelastic cross sections between 5 and 30 eV, and the data agree well with present results. The present results are in good agreement with the theoretical data of Shi *et al.* [27] beyond 100 eV, below which they are slightly higher compared to the present results. In contrast the theoretical data of Jain and Baluja [26] are higher than all the reported values below 20 eV and are lower compared to all data beyond 20 eV, but for energies above 500 eV they are in good agreement with the present results.

In Fig. 5 we report the total cross sections for e-PH_3 scattering along with previous experimental data. There is a paucity of experimental data for this molecule, and the only experimental data are that of Szmytkowski *et al.* [31]. A peak is observed in our data at 2.9 eV with a maximum value of cross section of around 48.0 $Å^2$, whereas the experimental data of Szmytkowski *et al.* [31] show a peak at 2.4 eV, and the peak value is 48.3 $Å^2$, which is very close to present calculations. Experimental data show a strong second peak around 5 eV, but we see this as more of a shoulder in our calculated data. There is good agreement in both shape and magnitude of the calculated and measured cross section above 10 eV.

Finally in Fig. 6 we report the total cross sections for e-PH_3 scattering along with other available theoretical data. Our low-energy cross sections predict a peak at a higher energy than the calculations of Bettega *et al.* [33] and Munjal and Baluja [32]. The theoretical data of Jain and Baluja [26] are, as in the case of H_2S, high compared to all reported data below 20 eV, beyond which is the data are lower than present data. However, at high energies their data tend to match with present results.

IV. CONCLUSION

In this paper we have sought to show that through the combination of two different electron-molecule-scattering codes (the *R*-matrix method using the Quantemol-N code for

low energies and the SCOP formalism at higher energies) it is possible to provide a set of reliable cross sections across a wide energy range (0.01 eV to 2 keV). We have illustrated this methodology for three simple polyatomic molecular targets NH_3, H_2S, and PH_3 for which there exists a good database against which we can benchmark our results. The results are promising since the two methods match at the transition energy (15 eV) and show good agreement with available data throughout the energy range. Therefore we may have confidence that the methodology we propose may be used to calculate such cross sections in other molecular systems and so may be used to estimate cross sections for electron scattering from molecular targets that cannot be easily studied experimentally (e.g., free radicals CF_x and SiH_x or OH). Such data are needed in a variety of applications from aeronomy to plasma modeling. Accordingly such a methodology maybe built into the design of online databases to provide a "data user" with the opportunity to request their own set of cross sections for use in their own research. Such a prospect will be explored by the emerging Virtual Atomic and Molecular Data Centre [60] [http://batz.lpma.jussieu.fr/www_VAMDC/].

ACKNOWLEDGEMENT

MVK thanks the Department of Science and Technology, New Delhi, for financial support through project No. SR/S2/LOP-26/2008, under which part of this work was done.

[1] M. Vinodkumar, C. G. Limbachiya, K. N. Joshipura, and N. J. Mason, Eur. Phys. J. D **61**, 579 (2011).
[2] L. G. Christophorou, *Electron-Molecule Interactions and Their Applications*, Vol. 1 (Academic Press, New York, 1982).
[3] L. Wallace and D. M. Hunten, Rev. Geophys. Space Phys. **16**, 289 (1978).
[4] L. S. Slobodkin, I. F. Buyakov, R. D. Cess, and J. Caldwell, J. Quant. Spectrosc. Radiat. Transfer **20**, 481 (1978).
[5] N. C. Jones, D. Field, S. L. Lunt, and J. P. Ziesel, Phys. Rev. A **78**, 042714 (2008).
[6] C. Szmytkowski, K. Maciag, G. Karwasz, and D. Fillipovic, J. Phys. B: At. Mol. Opt. Phys. **22**, 525 (1989).
[7] E. Bruche, Ann. Phys. (Leipzig) **1**, 93 (1929).
[8] D. Alle, R. Gulley, S. Buckman, and M. Brunger, J. Phys. B: At. Mol. Opt. Phys. **25**, 1533 (1992).
[9] A. Zecca, G. P. Karwasz, and R. S. Brusa, Phys. Rev. A **45**, 2777 (1992).
[10] O. Sueoka, S. Mori, and Y. Katayama, J. Phys. B: At. Mol. Opt. Phys. **20**, 3237 (1987).
[11] G. Garcia and F. Manero, J. Phys. B **29**, 4017 (1996).
[12] W. M. Ariyasinghe, T. Wijeratne, and P. Palihawadana, Phys. Res. B **217**, 389 (2004).
[13] H. Munjal and K. Baluja, Phys. Rev. A **74**, 032712 (2006).
[14] F. Gianturco, J. Phys. B: At. Mol. Opt. Phys. **24**, 4627 (1991).
[15] J. Yuan and Z. Zhang, Phys. Rev. A **45**, 4565 (1992).
[16] Y. Liu, J. Sun, Z. Li, Y. Jiang, and L. Wan, Z. Phys. D **42**, 45 (1997).
[17] A. Jain, J. Phys. B **21**, 905 (1988).
[18] M. L. Marconi, D. A. Mendis, A. Korth, R. P. Lin, D. L. Mitchell, and H. Reme, Astrophys. J. **352**, L17 (1990).
[19] Y. C. Minh, W. M. Irvine, D. McGonagle, and L. M. Ziurys, Astrophys. J. **360**, 136 (1990).
[20] R. J. Gulley, M. J. Brunger, and S. J. Buckman, J. Phys. B **26**, 2913 (1993).
[21] V. F. Sokolov and Y. A. Sokolova, Sov. Techn. Phys. Lett. **7**, 268 (1981).
[22] C. Szmytkowski, P. Mozejko, and A. Krzysztofowicz, Radiat. Phys. Chem. **68**, 307 (2003).
[23] M. Varella, M. Bettega, and M. Ferreira, J. Chem. Phys. **111**, 6396 (1999).
[24] M. Gupta and K. Baluja, Eur. Phys. J. D **41**, 475 (2007).
[25] B. H. Lengsfield, T. N. Rescigno, C. W. McCurdy, and S. Parker (private communication).
[26] A. Jain and K. Baluja, Phys. Rev. A **45**, 202 (1992).
[27] D. Shi, Y. Liu, J. Sun, X. Yang, and Z. Zhu, Chin. Phys. Soc. **14**, 2208 (2005).
[28] M. B. Parish, J. Elec. Chem. Soc. **127**, 2729 (1980).
[29] M. Y. Simmons, S. R. Schofield, J. L. O'Brien, N. J. Curson, L. Oberbeck, T. Hallam, and R. G. Clark, Surf. Sci. **532**, 1209 (2003).
[30] T. Encrenaz, B. B'ezard, J. Crovisier, A. Coustenis, E. Lellouch, S. Gulkis, and S. K. Atreya, Planet. Space Sci. **43**, 1485 (1995).
[31] C. Szmytkowski, L. Klosowski, A. Domaracka, M. Piotrowicz, and E. Ptasinska-Denga, J. Phys. B: At. Mol. Opt. Phys. **37**, 1833 (2004).
[32] H. Munjal and K. Baluja, J. Phys. B: At. Mol. Opt. Phys. **40**, 1713 (2007).
[33] M. Bettega, M. Lima, and L. Ferreira, J. Chem. Phys. **105**, 1029 (1996).
[34] M. Vinodkumar, K. Korot, and P. C. Vinodkumar, Eur. Phys. J. D **59**, 379 (2010).
[35] L.A. Morgan, J. Tennyson, and C. J. Gillan, Comput. Phys. Commun. **114**, 120 (1998).
[36] J. Tennyson, J. Phys. B : At. Mol. Opt. Phys. **29**, 6185 (1996).
[37] D. Bouchiha, J. D. Gorfinkiel, L. G. Caron, and L. Sanche, J. Phys. B: At. Mol. Opt. Phys. **40**, 1259 (2007).
[38] J. Tennyson, D. B. Brown, J. M. Munro, I. Rozum, H. N. Varambhia, and N. Vinci, J. Phys. Conf. Series **86**, 012001 (2007).
[39] A. M. Arthurs and A. Dalgarno, Proc. Phys. Soc. London, Sect. A **256**, 540 (1960).
[40] A. Faure, J. D. Gorfinkiel, L. A. Morgan, and J. Tennyson, Comput. Phys. Commun. **144**, 224 (2002).
[41] H. N. Varambhia, J. J. Munro, and J. Tennyson, Int. J. Mass Spectrom. **271**, 1 (2008).
[42] B. H. Bransden and C. J. Joachain, *Physics of Atoms and Molecules* (Pearson Education, New York, 2003).
[43] A. Jain and K. L. Baluja, Phys. Rev. A **45**, 202 (1992).
[44] A. Jain, Phys. Rev. A **34**, 3707 (1986).
[45] A. Jain, J. Phys. B **22**, 905 (1988).
[46] I. Gradashteyn and I. M. Ryzhik, *Tables of Integrals, Series and Products* (Associated Press, New York, 1980).

[47] C. F. Bunge, J. A. Barrientos, and A. V. Bunge, At. Data Nucl. Data Tables **53**, 113 (1993).
[48] S. Hara, J. Phys. Soc. Jpn. **22**, 710 (1967).
[49] X. Zhang, J. Sun, and Y. Liu, J. Phys. B: At. Mol. Opt. Phys. **25,** 1893 (1992).
[50] G. Staszewska, D. W. Schewenke, D. Thirumalai, and D. G. Truhlar, Phys. Rev. A **28**, 2740 (1983).
[51] M. Vinodkumar, C. Limbachiya, and H. Bhutadia, J. Phys. B **43**, 015203 (2010)
[52] M. Vinodkumar, R. Dave, H. Bhutadia, and B. Antony, Int. J. Mass Spectrom. **292**, 7 (2010).
[53] M. Vinodkumar, K. Korot, and H. Bhutadia, Int. J. Mass Spectrom. **294,** 54 (2010).
[54] National Institute of Standards and Technology, [http://srdata.nist.gov/cccbdb/].
[55] R. Greer and D. Thompson, J. Phys. B: At. Mol. Opt. Phys. **27**, 3533 (1994).
[56] D. R. Lidez, *CRC Handbook of Physics and Chemistry*, 74th ed. (Chemical Rubber Company, Boca Raton, FL, 1993–1994).
[57] R. Roberage and D. Salahub, J. Chem. Phys. **70**, 1177 (1979)
[58] S. K. Shih, S. D. Peyerimhoff, and R. J. Buenker, Chem. Phys. **17**, 391 (1976).
[59] G. Hertzberg, *Molecular Spectra and Molecular Structure* (D. Van Nostrand, New York, 1966).
[60] M. L. Dubernet *et al.*, J. Quant. Spectrosc. Rad. Transf. **111**, 2151 (2010).